Langmuir

Article

pubs.acs.org/Langmuir

Study of the Formation and Quick Growth of Thick Oxide Films Using Platinum Nanoelectrodes as a Model Electrocatalyst

Stephen J. Percival and Bo Zhang*

Department of Chemistry, University of Washington, Seattle, Washington 98195-1700, United States

Supporting Information

ABSTRACT: We report a study of the formation and quick growth of thick films of platinum oxide on platinum nanoelectrodes at low anodic potentials. Here, structurally well-defined platinum nanoelectrodes are used as a model platform for nanoscale platinum electrocatalysts. Platinum films are formed on the surface of the nanoelectrode upon application of a constant anodic potential in an acidic environment for an extended time period. A current spike is initially observed, which is attributed to capacitance charging, the oxidation of water, and the initial oxidation of the platinum surface. A finite residual current follows the initial current spike, which is composed of both water oxidation and the oxidation of platinum metal concealed beneath the growing oxide layer. These films are observed to be structurally irreversible, grow to be relatively thick, and protrude out of the glass insulating material encasing the nanoelectrode due to the added volume of the oxygen incorporated into the growing platinum oxide film. Once reduced, the platinum metal remains protruding out of the glass, and its presence is confirmed by both SEM imaging and cyclic voltammetry. Steady-state voltammetric data shows a finite increase in the diffusion-limited faradaic current of the nanoelectrode, relative to the initial steady-state current, after the oxidation/reduction of the platinum which is due to an increased area of the protruding platinum metal. A minimum apparent rate of ~1.2 nm/min can be calculated for the growth of the platinum oxide film. The use of platinum nanoelectrodes has shown several distinct advantages in this study, including better control of the size and morphology of the individual electrocatalysts, the ability to image using electron microscopy, and the ability to use voltammetry to evaluate the geometry of the electrode quickly.

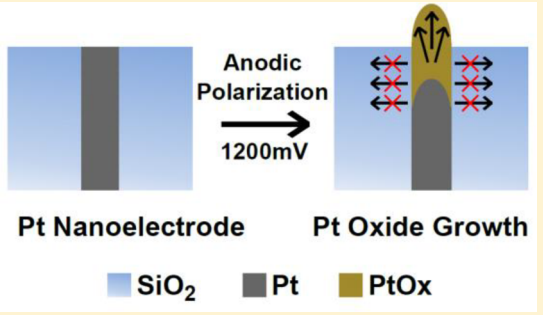

INTRODUCTION

Platinum is one of the most active electrocatalytic materials for numerous key reactions in energy conversion and storage.[1−5] Some reactions, including the oxygen evolution reaction (OER),[6,7] take place at high applied anodic potentials while others, such as the oxidation of methanol,[8] hydrazine,[9,10] and borohydride,[11,12] take place under more mild conditions and are all relevant to fuel cell operation. The kinetics of these oxidation reactions can be strongly affected by the presence of surface metal oxides.[6,10] Understanding the oxidation behavior of such catalysts at oxidizing potentials is important for fully understanding the kinetics of the catalytic reactions.[1,6,13]

The oxidation of bulk platinum metal has been extensively studied and has resulted in many great contributions although the process is still not fully understood.[1,14] It has been demonstrated that thick platinum oxide can form under conditions of high galvanostatic current densities[15] or high potentiostatic anodization.[16] Other studies have also shown that the oxide layer thickness can be increasingly grown with a fast potential cycling[17,18] or under very harsh conditions.[15,19] Conway and coworkers have shown that the formation of different oxides can be independent of one another where the typically formed thin oxide (also known as α-oxide) could be selectively reduced and reformed without reducing the thick oxide layer (also known as β-oxide), implying that the thin oxide formed on the metal surface beneath the thick oxide layer.[20,21] Biegler and Woods[22] reached the conclusion that even at high anodic potentials (2.98 V vs NHE) a limit of 2.66 oxygen atoms/platinum atom is achieved with only monolayer coverage and was later supported using ellipsometry by Parsons and Visscher.[23] Later Conway and coworkers demonstrated that a thick platinum oxide layer can be grown without limits to the thickness of the film when the applied potential exceeds 1.9 V (vs NHE) for extended periods of time (>12 h) and that oxide growth follows a direct logarithmic growth law with time at a constant potential.[1,24,25] Recently it has been determined that the growth of oxide on platinum is limited to a few monolayers at anodic potentials of up to 1.50 V.[26]

Typically these studies do not observe or discuss the growth of thick platinum oxide layers by holding the electrode potential at relatively low anodic potentials. However, many materials exhibit different properties when scaled down to nanometer dimensions.[27] One excellent example is the recent study reported by Mirkin and coworkers on the dissolution of platinum on nanoscale platinum electrodes at moderately negative cathodic potentials during the oxygen reduction

Received: June 13, 2014
Revised: August 22, 2014
Published: August 27, 2014

reaction (ORR).[28] The growth of platinum oxides resulting in the loss of the electrochemically active surface area can impact fuel cell operation utilizing platinum nanoparticles by inhibiting the catalytic reaction on the oxide surface.[28−30]

Here, we report on the growth of thick platinum oxide films under relatively low anodic polarization potentials on platinum electrodes of nanoscale dimensions. This platform can be thought of as a model for platinum nanocatalysts with implications for fuel cell operation where even at lower operating potentials there may be an unwanted formation of oxidized films on the platinum nanocatalyst, reducing its efficiency. The growth of these films on platinum nanoelectrodes appears to be much faster than previously reported and in fact can be observed directly through electron microscopy (EM). The use of EM and electrochemistry has enabled us to obtain an apparent growth rate of the platinum oxide, which exceeds any growth rate documented to date that we are aware of. In addition, the oxide film exhibits signs that it may be soft/malleable with a high degree of structural irreversibility.

EXPERIMENTAL SECTION

Chemicals and Materials. All aqueous solutions were prepared using deionized water (>18 MΩ cm) produced in a Barnstead Nanopure water purification system. Ferrocene methanol (FcMeOH, Aldrich, 97%), anhydrous sodium sulfate (Na_2SO_4, J. T. Baker), sulfuric acid (H_2SO_4, Fisher), argon (Ar, Praxair, >99%), and a Pt microwire (25 μm diameter, Alfa Aesar, 99.99%) were all used as received from the manufacturers.

Electrochemical Measurements. Electrochemical data was recorded using a computer-controlled Dagan Chem-Clamp voltammeter/amperometer, and data was recorded using an in-house virtual instrumentation program written in LabView (National Instruments) on a desktop PC equipped with a PCI-6251(National Instruments) data acquisition card. A Hg/Hg_2SO_4 reference electrode (CH Instruments, Inc.) was used for all CVs, and experimental CV data was manually baseline corrected. The Hg/Hg_2SO_4 reference electrode was used to prevent chloride contamination, which is known to block platinum oxidation at lower potentials.[31] All potentials presented are referenced to a Ag/AgCl reference electrode unless otherwise noted. Sulfuric acid solutions were bubbled with argon for >30 min prior to use to ensure that the solution was free of dissolved oxygen before anodic polarization. All experiments were done at room temperature.

Scanning Electron Microscopy (SEM) and Energy-Dispersive X-ray Spectroscopy (EDS). SEM images were obtained using a field-emission microscope (FEI Sirion) equipped with a through-the-lens secondary electron detector with a resolution of 1 to 3 nm at the Nanotech User Facility located at the University of Washington. All samples were sputter coated with a 2 to 3 nm conducting layer of gold/palladium or carbon prior to SEM imaging. EDS data was obtained using an Oxford X-max 80 mm^2 silicon drift detector.

RESULTS AND DISCUSSION

Fabrication and Characterization of Platinum Nanoelectrodes. The procedure for preparing the platinum disk nanoelectrodes is described in detail elsewhere.[32−34] However, to briefly summarize, a 25-μm-diameter platinum wire was placed in a fused silica capillary tube (o.d. 1 mm, i.d. 0.3 mm, Sutter Instrument Co.), and one end was sealed using an oxygen/hydrogen flame. The fused silica capillary was then placed in a P-2000 laser pipet puller (Sutter Instrument Co.), and vacuum was applied to the unsealed end of the capillary. The laser was used to heat and seal the fused silica around the platinum without pulling the capillary. Then the platinum/fused silica assembly was pulled (pull parameters: heat = 750, filament = 2, velocity = 60, delay = 140, pull = 250), resulting in two ultrasharp tips with the platinum nanowires sealed inside. The tips were then electrically contacted using tungsten wires and conductive silver paste (DuPont). To expose the electrodes, a high-speed beveling process was employed by utilizing a diamond lapping film (3M, 0.5 μm diamonds, Ted Pella Inc.) attached to a rapidly rotating wheel (7500 rpm). The electrode was polished by slowly approaching the wheel while visually monitoring using an inverted optical microscope.

The platinum nanoelectrodes were characterized by SEM and steady-state cyclic voltammetry. The polished platinum nanoelectrodes are flush with the glass insulating layer, as shown in Figure 1. The platinum nanoelectrode shown in

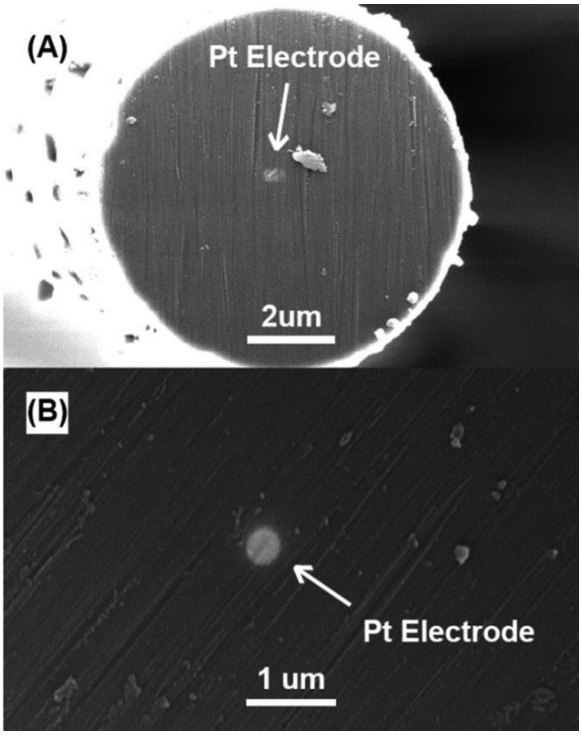

Figure 1. (A, B) SEM images of freshly polished Pt nanoelectrodes showing the electrode surfaces flush with the glass insulator.

Figure 1A located at roughly the center of the glass tip is not perfectly round but more oval-shaped. Figure 1B shows a more uniformly shaped platinum electrode with a diameter of less than 500 nm.

Figure 2A shows the voltammetric response of two platinum nanoelectrodes in 2 mM ferrocene methanol (FcMeOH), one having a radius of 219 nm and the other 122 nm (calculated from eq 1). Both electrodes show a sigmoidally shaped CV response typical of a conventional UME of this size.[35] The diffusion-limited steady-state currents of the electrodes were then used to calculate the radii of the electrodes using the steady-state current equation for a planar disk UME electrode[33−35]

$$i_{ss} = 4nFDCr \quad (1)$$

where n is the number of electrons transferred per redox molecule, F is the Faraday constant, D is the diffusion coefficient of the redox molecule (for FcMeOH, $D = 6.7 \times 10^{-6}$ cm^2/s),[36] C is the bulk concentration of the redox molecule, and r is the radius of the electrode. The steady-state

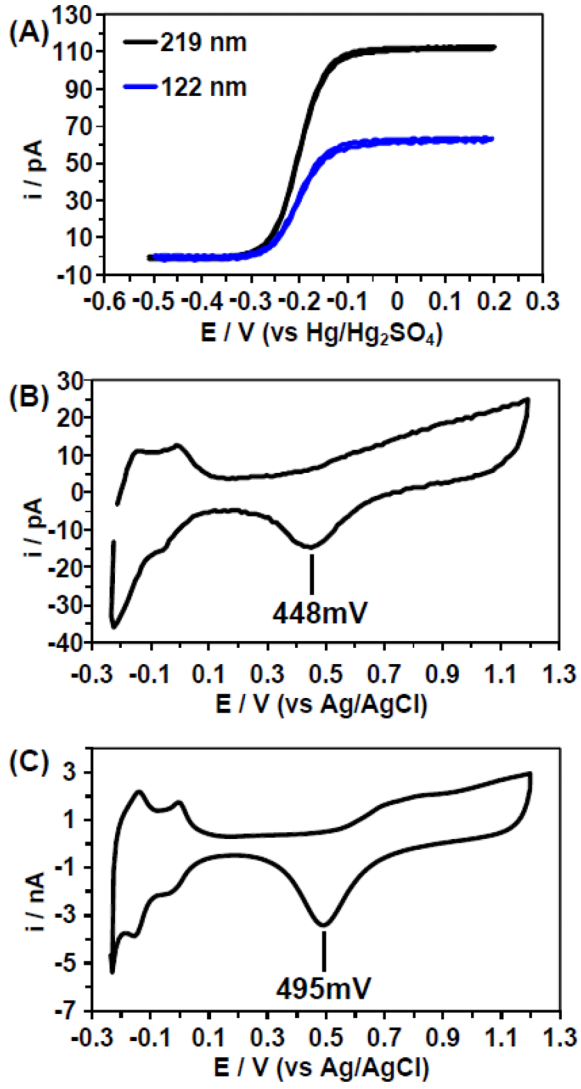

Figure 2. (A) CVs of two platinum nanoelectrodes with different radii in 2 mM FcMeOH with 100 mM Na_2SO_4 at a 50 mV/s scan rate and (B) a 124-nm-radius Pt nanoelectrode in 0.5 M H_2SO_4 at a 100 mV/s scan rate and (C) a 25-μm-diameter Pt electrode in 0.5 M H_2SO_4 at a 100 mV/s scan rate.

CVs were not only used to determine the sizes of the electrodes but are also used to determine any general changes to the area of the electrodes because an increase in the diffusion-limited current indicates an increase in the radius and geometric area of the electrode.

Sulfuric acid scans of the platinum electrode were used to determine the regions of platinum oxidation/reduction as well as the relative cleanliness of the platinum surface after exposure. A representative scan from a 124-nm-radius nanoelectrode is shown in Figure 2B and a 25-μm-diameter Pt UME in Figure 2C. The hydrogen adsorption/desorption peaks are observed at potentials below 100 mV (vs Ag/AgCl) on the forward and backward scans, respectively.[35,37] These peaks are from the adsorption/desorption of hydrogen ions in solution on the platinum surface and closely match the representative sulfuric acid scan of the 25 μm Pt UME. Also seen in the sulfuric acid scan for the nanoelectrode is an increase in current during the anodic sweep starting at approximately 500 mV and continuing to increase until the sweep reverses. This is slightly different from the 25 μm Pt UME electrode where two distinct current increases are observed, one starting at ~570 mV which increases and plateaus to a steady current and another current increase located at approximately 940 mV. These current increases are due to the oxidation of the platinum surface forming platinum oxides initially in the form of an adsorbed layer of oxygen followed by the formation of the submonolayer coverage of PtO.[14] In the case of the 25 μm Pt UME, the second increase, starting at 940 mV, may possibly be attributed to the onset of an interfacial place exchange whereby the oxygen ions in the PtO, initially formed at lower potentials, exchange positions with platinum atoms in the metal surface forming a bilayer PtO structure.[14] During the cathodic sweep, a single large peak is observed (in addition to the hydrogen peaks at lower potentials) centered at ~500 mV which is due to the reduction of the compact α-oxide layer, formed during the anodic sweep.[1,21] Interestingly, the reduction peak for the nanoelectrode in Figure 2B is centered at ~450 mV, indicating that the oxide film formed on the nanoelectrode is more electrochemically irreversible and requires a lower potential for reduction during the cathodic sweep. Additionally, the nanoelectrode surface may also undergo oxidation with an increased rate of initial oxide formation and place exchange at a given potential, and the different oxidation mechanisms may proceed at lowered potentials compared to that of bulk platinum. This can be seen in sulfuric acid scans where the initial oxidation current for the nanoelectrode begins at a lower potential than the 25 μm Pt UME and also does not level off but continues to increase with increasing potential. The ~47 mV lower potential needed to reduce the oxide and the increasing oxidation with the anodic potential sweep on the nanoelectrode may be due to the increased adsorption energy of oxygen to the platinum surface of the nanoelectrode as compared to a bulk platinum surface and has been previously observed with other platinum nanostructures.[27,38−40] The magnitude of the potential shift for the oxide reduction peak for a nanoelectrode of that diameter was unexpected but smaller than some reported shifts for small-diameter Pt nanoparticles.[27,38] This effect might be enhanced by the specific crystal faces present at the electrode surface where for a given specific crystal orientation the oxide reduction peak will shift to more negative potentials but will also shift the onset of oxide formation in the positive direction.[41]

Oxidation of the platinum by anodic polarization was accomplished by first holding the electrode at 0 mV vs Ag/AgCl in argon-bubbled 0.5 M H_2SO_4 and then quickly stepping it up to a 1200 mV potential where the electrode was held for the duration of the oxidation experiment. If the electrode was reduced after the oxidation, then the potential was stepped back to 0 mV. The most prominent feature from the potential step current−time trace is the large current spike, called the peak current, and can be seen in Figure 3A. This current−time trace is obtained from a 100-nm-radius electrode stepped to 1200 mV and shows a peak current spike of ~2.8 nA that quickly decays to a steady residual current of ~38 pA larger than the original baseline current. The residual current from the current−time trace is taken as the average current 5 min after the potential step and has contributions from both the OER as well as the oxidation of platinum. The residual current measurement was taken after 5 min in order to give a fairly accurate result of the differences between the potential steps while not allowing sufficient time to change the electrode surface drastically. Figure 3B shows how the peak current changes with potential when the nanoelectrode is stepped from

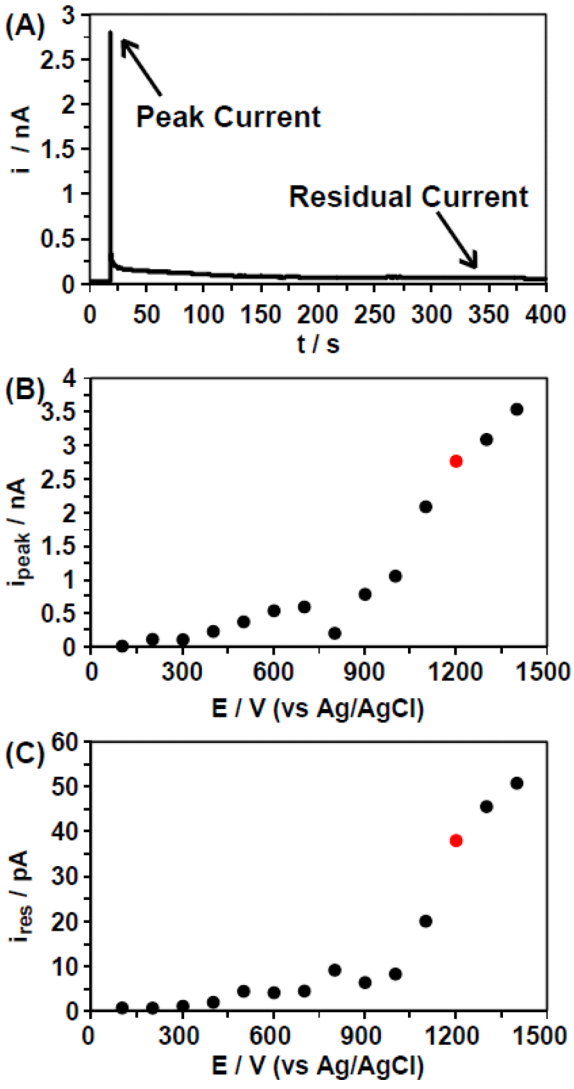

Figure 3. (A) Potential step chronoamperometric trace at 1200 mV from a 100-nm-radius Pt nanoelectrode in 0.5 M H_2SO_4 where the initial peak current (red dot in (B)) is observed to decay to a nonzero residual current (red dot in (C)). (B) Peak current observed at each potential step and (C) residual current observed for each potential step measured as the average current 5 min after the potential step. All potential steps were recorded using the same electrode.

0 mV to a given positive potential. It is expected that the peak current increases as the potential steps are increased due to the double-layer capacitance charging at the surface of the electrode.[35]

There is a small increase in the peak current as the stepping potential is increased to ~500−600 mV, but essentially there is very little change until the stepping potential reaches 1100 mV, where a larger increase is observed. The small increase observed at 500−600 mV may be due to the onset of platinum oxidation which is assumed to be limited to sub- or monolayer thicknesses but has a slow growth rate at low potentials.[1,25] This is also observed with the residual currents, shown in Figure 3C, where again the current essentially does not increase until the stepping potential is 1100 mV or above. At that potential, it is apparent that there is an increase in the rate of the platinum oxidation reaction or possibly a new reaction has started. At 1200 mV, there is again a large increase in residual current compared to the previous step, but as the potential is stepped higher, the currents increase less dramatically. The OER is expected to contribute to the current at these increased potentials, but its rate is dependent on the pH of the solution.[42] In a sufficiently acidic solution, the OER would not proceed at a significant rate until a high potential was reached.[43] Nonetheless, it would still be present when platinum oxidation is occurring, making it difficult to determine the specific current that can be attributed to the platinum oxidation. The residual current increase observed at 1100 mV may be due to the onset of multilayer platinum oxidation at a potential much lower than previously described.[1]

Figure 4A,B shows the results of the oxidation of a platinum nanoelectrode held at 1200 mV for 90 min and removed from 0.5 M H_2SO_4 while still under anodic polarization in order to prevent the reduction of oxidized platinum. The SEM images clearly show the growth of the electrode and the protrusion out of the surrounding glass insulation. Energy dispersive X-ray spectroscopy (EDS) measurements of this electrode are shown

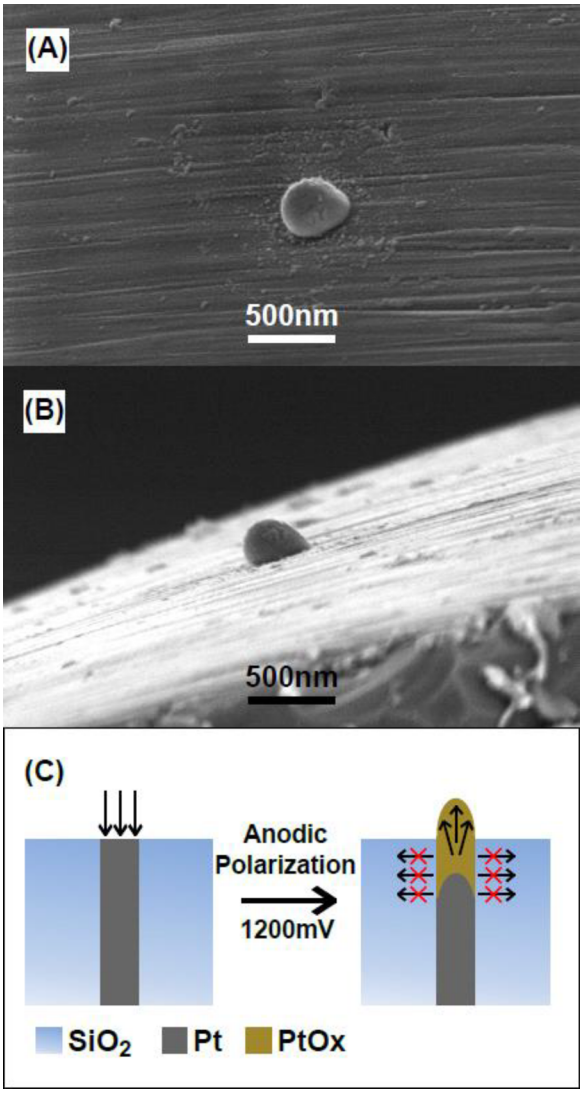

Figure 4. (A) SEM image of an electrode after anodic oxidation at 1200 mV for 90 min. (B) Side view of the same electrode as in (A) showing the protruding nature of the Pt oxide growth. (C) Schematic showing the hypothesized growth of the Pt oxide where the surrounding glass insulation forces the increasing volume of Pt oxide to grow out of the glass pore in a radial direction.

in Supporting Information Figure S3 and verify that the protrusion is indeed the platinum nanoelectrode. A representation of what we believe is physically occurring as the platinum oxide is growing and expanding can be seen in the schematic in Figure 4C. The schematic illustrates that the platinum electrode is encased in a rigid insulator and that the increasing volume resulting from the platinum oxide formation causes the soft film to protrude out of the insulator, forming a rounded hemispherical structure. Previous studies have found that there is a possibility of surface reactions occurring on the sidewall of a glass-sealed Pt nanowire.[44,45] Platinum oxidation and film growth would certainly occur at the Pt/glass interface but would expand and constrict the opening, limiting the growth rate. If there was a substantial contribution from PtOx growth on the sides of the nanowire where the Pt/glass interface is located, then we would expect to see a more ringlike structure protruding from the glass instead of the rounded, centrally located structure observed in the SEM images. However, the schematic illustrates the additional effect of oxide growth into the nanowire from the sides or an increased growth rate from the edges of the electrode causing the oxide to grow radially into the Pt nanowire, but the fact remains that we do not know exactly what is occurring within the nanowire. The bulk growth and resulting protrusion of the oxidized platinum are due to the increasing volume of the platinum oxide as oxygen atoms are incorporated into the crystal lattice of platinum through the previously discussed interfacial place-exchange mechanism.[14] Additionally as the oxide layer thickens and the oxygen is incorporated into the lattice structure, there may be a formation of voids from the buckling of the platinum atoms, further expanding the oxide layer and possibly causing some instability of the oxide film.[46]

If this platinum oxide film is reduced after it has grown out of the glass insulation, then the surface area is found to increase due to the highly irreversible processes that take place as the oxide film is growing. Figure 5A,B shows SEM images of a Pt nanoelectrode that had been oxidized for 60 min at 1200 mV and then reduced by switching the potential back to 0 mV. The images show that the electrode is protruding out of the glass insulating layer, and its surface appears rougher, or faceted, compared to the electrode shown in Figure 4. The increase in geometric surface area exposed to the redox solution would increase the resulting steady-state current after the oxidation and reduction of the platinum surface. This can be seen in Figure 5C. The limiting current for the electrode before the oxidation/reduction step is ~125 pA, yielding a calculated radius of 241.8 nm when eq 1 is used, closely matching the SEM measured radius of ~227 nm. After the oxidation/reduction step, the current increases to ~187 pA and the CV exhibits sudden current fluctuations (increasing and decreasing) that may be due to a somewhat porous and unstable nature of the reduced platinum, where perhaps small particles become dislodged and/or new areas become available for the redox reaction. This can be seen in the SEM images, where small particulates are littering the area around the protruding nanoelectrode. The incorporation of oxygen into the growing oxide film and possible void formation, discussed earlier, results in highly structurally irreversible oxide growth. Upon reduction, platinum is unable to reform a compact and uniform crystal structure, resulting in the rough and unstable surface observed in the SEM image.

The method of steady-state cyclic voltammetry also allows for the determination of an approximate growth rate for the

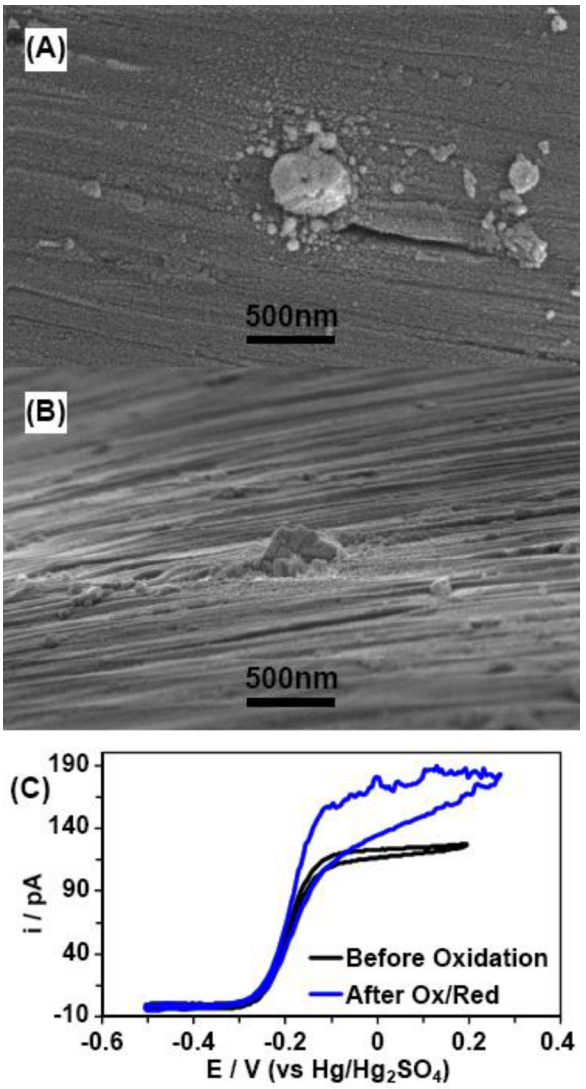

Figure 5. (A, B) SEM images of an electrode oxidized for 60 min at 1200 mV and then reduced at 0 mV showing the more crystalline (faceted) nature of the Pt surface. (C) CVs in 2 mM FcMeOH before and after the oxidation/reduction step showing an increase in the limiting current (100 mM Na_2SO_4 supporting electrolyte, 50 mV/s scan rate).

platinum oxide film. By using a platinum electrode where the disk surface is initially recessed into the quartz insulator and measuring the increase in the diffusion-limited steady-state current, a change in the recessed depth can be calculated using eq 2[47−49]

$$i_{ss} = \frac{4\pi nFDCr^2}{4L + \pi r} \quad (2)$$

where the constants are the same as previously defined for eq 1 and L represents the depth of the electrode recess. Figure 6A again shows an SEM image of a 142-nm-radius platinum nanoelectrode that has been oxidized at 1200 mV for 90 min and then reduced at 0 mV. Figure 6B shows the same electrode but is tilted to show the recessed depth of the electrode that is clearly recessed into the quartz. The radius of the electrode was measured from the SEM images and used with the steady-state current of ~18.8 pA in the 2 mM FcMeOH solution to

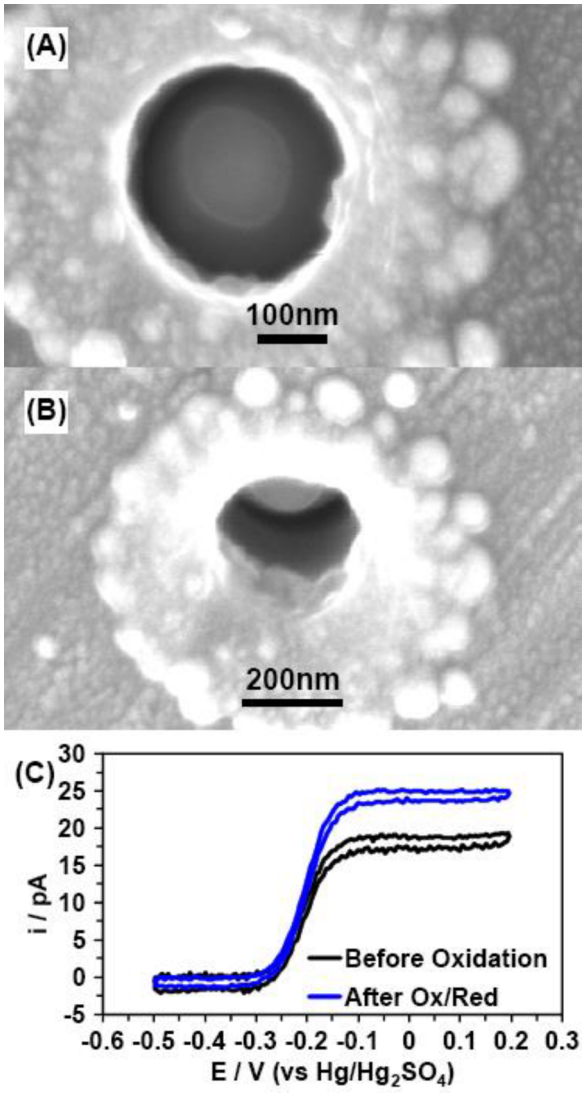

Figure 6. (A, B) SEM images of a recessed platinum nanoelectrode that was oxidized for 90 min at 1200 mV and then reduced at 0 mV. The SEM image in (B) is at a tilted angle to show the electrode surface and the sidewall of the recess. (C) CVs from the electrode shown in (A) and (B) showing the steady-state currents before oxidation and after oxidation where the increased current indicates a less-recessed electrode surface.

calculate an initial depth of ~324 nm before the oxidation procedure.

After the oxidation and reduction, an increased steady-state current of ~25.0 pA was used to obtain a final recessed depth of ~217 nm. The calculated depth closely matches the SEM-measured value of ~204 nm, which was measured at an angled view. This means that the electrode increased in volume to fill in 107 nm (~33% of the recessed depth) and gives a lower limit of the oxide film growth to be ~1.2 nm/min for this particular electrode. We call this a lower limit because we assume that some volume may have been lost due to the reduction step whereby some oxygen would be driven out of the crystal lattice, thus decreasing the total volume. This electrochemically calculated value is comparable to an average growth rate of 1.58 ± 0.99 nm/min which was obtained from visually measuring the PtOx protruding from the glass insulators. The electrochemically calculated rate is lower than the visually measured rate possibly because of the recessed nature of the nanoelectrode which can hinder the mass transport. The increased mass-transfer resistance means that the acidic protons generated from the OER would have more difficulty diffusing away from the electrode and could lower the local pH, making the Pt oxidation less favorable at the electrode surface, slowing the oxide growth. Interestingly, after the reduction of this oxide, the steady-state redox CV did not exhibit much variation in current, which may be due to oxide layer growth confined by the quartz insulator limiting its growth to just one direction. When reduced, the oxide layer was able to form a more compact structure as compared to that in Figure 5, where the protrusion allowed it to grow radially outward, thus increasing the disorder and making it more difficult to realign its crystal structure upon reduction.

It is apparent that the platinum oxidation on nanoscale electrodes is not limited to a few monolayers, and questions remain regarding why the oxide growth differs from that of bulk platinum. We will continue to investigate this interesting result. The growth of thick oxide films on platinum nanoelectrodes at relatively low anodic potentials may be indicative of intrinsic stress in the platinum crystal structure where the growth of the oxide layer is facilitated by the higher strain energy. The growth rate of the thick platinum oxide may also be largely dependent on the crystal face present on the surface of the electrode, and a few studies have stated that crystal faces will influence the oxide growth rate.[24] We feel it important to note that the growth of thick oxide films is not always observed and that surface contaminants, likely from the polishing step, may hinder the growth process.

■ CONCLUSIONS

We have investigated the growth of thick platinum oxide films on platinum nanoelectrodes at low anodic holding potentials. The potential step experiments reveal a critical potential where the residual current at the nanoelectrode increases due to both the onset of platinum oxidation and the OER. The growth of the oxide causes the growing film to protrude out of the glass insulator, indicating the soft nature of the film. The diffusion-limited steady-state current measurements of a simple redox molecule were used to evaluate the minimal growth rate of the oxide film in a recessed platinum nanoelectrode. It appears that the growth rate can be as high as 1.2 nm/min at a 1200 mV (vs Ag/AgCl) hold potential. This may be a consequence of the nanoscale dimensions of these platinum electrodes where the oxygen adsorption energy is increased compared to that of bulk platinum and may explain why the oxidation behavior and the subsequent growth of the oxide film are different from those of bulk platinum electrodes. Further investigation is needed to evaluate the growth rate more accurately and also to determine the nature of the oxide film that is grown by this method.

■ ASSOCIATED CONTENT

Supporting Information

SEM images of the electrode used in the potential step experiment with the before and after redox diffusion-limited CVs. SEM images of electrodes held at lower potentials showing little to no growth. EDS color plots of the oxidized electrode bulging out of the glass insulator seen in Figure 4. Measured SEM image of the electrode shown in Figure 6. Additional SEM images showing the reproducibility of oxide growth. This material is available free of charge via the Internet at http://pubs.acs.org.

AUTHOR INFORMATION

Corresponding Author

*Phone: (206) 543 1767. E-mail: zhang@chem.washington.edu.

Notes

The authors declare no competing financial interest.

ACKNOWLEDGMENTS

We gratefully acknowledge financial support from the AFOSR MURI (FA9550-14-1-0003). Part of this work was conducted at the University of Washington NanoTech User Facility, a member of the National Science Foundation, National Nanotechnology Infrastructure Network (NNIN). B.Z. is a recipient of the Sloan Research Fellowship.

REFERENCES

(1) Conway, B. E. Electrochemical Oxide Film Formation at Noble Metals as a Surface-Chemical Process. *Prog. Surf. Sci.* **1995**, *49*, 331−452.

(2) Marković, N. M.; Gasteiger, H. A.; Ross, P. N., Jr. Oxygen Reduction on Platinum Low-Index Single-Crystal Surfaces in Sulfuric Acid Solution: Rotating Ring-Pt(*hkl*) Disk Studies. *J. Phys. Chem.* **1995**, *99*, 3411−3415.

(3) Bockris, J. O'M.; Shamshul Huq, A. K. M. The Mechanism of the Electrolytic Evolution of Oxygen on Platinum. *Proc. R. Soc. London, Ser. A* **1956**, *237*, 277−296.

(4) Conway, B. E.; Ping, G. Surface Electrochemistry of the Anodic Cl_2 Evolution Reaction at Pt. Influence of Co-deposition of Surface Oxide Species on Adsorption of the Cl^- Intermediate. *J. Chem. Soc., Faraday Trans.* **1990**, *86*, 923−930.

(5) Alia, S. M.; Pivovar, B. S.; Yan, Y. Platinum-Coated Copper Nanowires with High Activity for Hydrogen Oxidation Reaction in Base. *J. Am. Chem. Soc.* **2013**, *135*, 13473−13478.

(6) Conway, B. E.; Liu, T.-C. Characterization of Electrocatalysis in the Oxygen Evolution Reaction at Platinum by Evaluation of Behavior of Surface Intermediate States at the Oxide Film. *Langmuir* **1990**, *6*, 268−276.

(7) Miles, M. H.; Klaus, E. A.; Gunn, B. P.; Locker, J. R.; Serafin, W. E.; Srinivasan, S. The Oxygen Evolution Reaction on Platinum, Iridium, Ruthenium and their Alloys at 80°C in Acid Solutions. *Electrochim. Acta* **1978**, *23*, 521−526.

(8) Childers, C. L.; Huang, H.; Korzeniewski, C. Formaldehyde Yields from Methanol Electrochemical Oxidation on Carbon-Supported Platinum Catalysts. *Langmuir* **1999**, *15*, 786−789.

(9) Roy, C.; Bertin, E.; Martin, M. H.; Garbarino, S.; Guay, D. Hydrazine Oxidation at Porous and Preferentially Oriented {100} Pt Thin Films. *Electrocatal.* **2013**, *4*, 76−84.

(10) Aldous, L.; Compton, R. G. The Mechanism of Hydrazine Electro-Oxidation Revealed by Platinum Microelectrodes: Role of Residual Oxides. *Phys. Chem. Chem. Phys.* **2011**, *13*, 5279−5287.

(11) Zhou, H.; Fan, F.-R.; Bard, A. J. Observation of Discrete Au Nanoparticle Collisions by Electrocatalytic Amplification Using Pt Ultramicroelectrode Surface Modification. *J. Phys. Chem. Lett.* **2010**, *1*, 2671−2674.

(12) Gyenge, E. Electrooxidation of Borohydride on Platinum and Gold Electrodes: Implications for Direct Borohydride Fuel Cells. *Electrochim. Acta* **2004**, *49*, 965−978.

(13) Jerkiewicz, G.; Borodzinski, J. J. Relation Between the Surface States of Oxide Films at Rh Electrodes and Kinetics of the Oxygen Evolution Reaction. *J. Chem. Soc., Faraday Trans.* **1994**, *90*, 3669−3675.

(14) Jerkiewicz, G.; Vatankhah, G.; Lessard, J.; Soriaga, M. P.; Park, Y.-S. Surface-Oxide Growth at Platinum Electrodes in Aqueous H_2SO_4 Reexamination of its Mechanism Through Combined Cyclic-Voltammetry, Electrochemical Quartz-Crystal Nanobalance, and Auger Electron Spectroscopy Measurements. *Electrochim. Acta* **2004**, *49*, 1451−1459.

(15) Shibata, S. The Activation of Platinum Electrodes by Preoxidation. *Bull. Chem. Soc. Jpn.* **1963**, *36*, 525−527.

(16) Shibata, S.; Sumino, M. P. Growth of Multilayer Oxide Films on Platinum Electrodes by Potentiostatic Anodization in Sulfuric Acid Solution. *Electrochim. Acta* **1971**, *16*, 1089−1098.

(17) Farebrother, M.; Goledzinowski, M.; Thomas, G.; Birss, V. I. Early Stages of Growth of Hydrous Platinum Oxide Films. *J. Electroanal. Chem.* **1991**, *297*, 469−488.

(18) Burke, L. D.; Roche, M. B. C. Hydrous Oxide Formation on Platinum − A Useful Route to Controlled Platinization. *J. Electroanal. Chem.* **1984**, *164*, 315−334.

(19) Shibata, S.; Sumino, M. P. Growth of Oxide Layers on Platinum Electrodes in Molten Alkali Nitrates. *Electrochim. Acta* **1975**, *20*, 871−876.

(20) Conway, B. E.; Tremiliosi-Filho, G.; Jerkiewicz, G. Independence of Formation and Reduction of Monolayer Surface Oxide on Pt from Presence of Thicker Phase-Oxide Layers. *J. Electroanal. Chem.* **1991**, *297*, 435−443.

(21) Jerkiewicz, G.; Tremiliosi-Filho, G.; Conway, B. E. Significance of the Apparent Limit of Anodic Oxide Film Formation at Pt: Saturation Coverage by the Quasi Two-Dimensional State. *J. Electroanal. Chem.* **1992**, *334*, 359−370.

(22) Biegler, T.; Woods, R. Limiting Oxygen Coverage on Smooth Platinum Anodes in Acid Solution. *J. Electroanal. Chem.* **1969**, *20*, 73−78.

(23) Parsons, R.; Visscher, W. H. M. An Ellipsometric Investigation of Adsorbed Layers on Platinum Electrodes at High Anodic Potentials. *J. Electroanal. Chem.* **1972**, *36*, 329−336.

(24) Tremiliosi-Filho, G.; Jerkiewicz, G.; Conway, B. E. Characterization and Significance of the Sequence of Stages of Oxide Film Formation at Platinum Generated by Strong Anodic Polarization. *Langmuir* **1992**, *8*, 658−667.

(25) Conway, B. E.; Barnett, B.; Angerstein-Kozlowska, H.; Tilak, B. V. A Surface-Electrochemical Basis for the Direct Logarithmic Growth Law for Initial Stages of Extension of Anodic Oxide Films Formed at Noble Metals. *J. Chem. Phys.* **1990**, *93*, 8361−8373.

(26) Alsabet, M.; Grden, M.; Jerkiewicz, G. Comprehensive Study of the Growth of Thin Oxide Layers on Pt Electrodes Under Well-Defined Temperature, Potential, and Time Conditions. *J. Electroanal. Chem.* **2006**, *589*, 120−127.

(27) Reier, T.; Oezaslan, M.; Strasser, P. Electrocatalytic Oxygen Evolution Reaction (OER) on Ru, Ir, and Pt Catalysts: A Comparative Study of Nanoparticles and Bulk Materials. *ACS Catal.* **2012**, *2*, 1765−1772.

(28) Noël, J.-M.; Yu, Y.; Mirkin, M. V. Dissolution of Pt at Moderately Negative Potentials During Oxygen Reduction in Water and Organic Media. *Langmuir* **2013**, *29*, 1346−1350.

(29) Holby, E. F.; Morgan, D. Application of Pt Nanoparticle Dissolution and Oxidation Modeling to Understanding Degradation in PEM Fuel Cells. *J. Electrochem. Soc.* **2012**, *159*, B578−B591.

(30) Imai, H.; Izumi, K.; Matsumoto, M.; Kubo, Y.; Kato, K.; Imai, Y. In Situ and Real-Time Monitoring of Oxide Growth in a Few Monolayers at Surfaces of Platinum Nanoparticles in Aqueous Media. *J. Am. Chem. Soc.* **2009**, *131*, 6293−6300.

(31) Zolfaghari, A.; Conway, B. E.; Jerkiewicz, G. Elucidation of the Effects of Competitive Adsorption of Cl^- and Br^- Ions on the Initial Stages of Pt Surface Oxidation by Means of Electrochemical Nanogravimetry. *Electrochim. Acta* **2002**, *47*, 1173−1187.

(32) Katemann, B. B.; Schuhmann, W. Fabrication and Characterization of Needle-Type Pt-Disk Nanoelectrodes. *Electroanalysis* **2002**, *14*, 22−28.

(33) Li, Y.; Bergman, D.; Zhang, B. Preparation and Electrochemical Response of 1-3 nm Pt Disk Electrodes. *Anal. Chem.* **2009**, *81*, 5496−5502.

(34) Shao, Y.; Mirkin, M. V.; Fish, G.; Kokotov, S.; Palanker, D.; Lewis, A. Nanometer-Sized Electrochemical Sensors. *Anal. Chem.* **1997**, *69*, 1627−1634.

(35) Bard, A. J.; Faulkner, L. R. *Elecrochemical Methods*, 2nd ed.; John Wiley & Sons: New York, 2001.

(36) Anicet, N.; Bourdillon, C.; Demaille, C.; Moiroux, J.; Savéant, J.-M. Catalysis of the Electrochemical Oxidation of Glucose by Glucose Oxidase and a Single Electron Cosubstrate: Kinetics in Viscous Solutions. *J. Electroanal. Chem.* **1996**, *410*, 199−202.
(37) Climent, V.; Feliu, J. M. Thirty Years of Platinum Single Crystal Electrochemistry. *J. Solid. State. Electrochem.* **2011**, *15*, 1297−1315.
(38) Mayrhofer, K. J. J.; Blizanac, B. B.; Arenz, M.; Stamenkovic, V. R.; Ross, P. N.; Markovic, N. M. The Impact of Geometric and Surface Electronic Properties of Pt-Catalysts on the Particle Size Effects in Electrocatalysis. *J. Phys. Chem. B* **2005**, *109*, 14433−14440.
(39) Percival, S. J.; Zhang, B. Electrocatalytic Reduction of Oxygen at Single Platinum Nanowires. *J. Phys. Chem. C* **2013**, *117*, 13928−13935.
(40) Speder, J.; Altmann, L.; Bäumer, M.; Kirkensgaard, J. J. K.; Mortensen, K.; Arenz, M. The Particle Proximity Effect: From Model to High Surface Area Fuel Cell Catalysts. *RSC Adv.* **2014**, *4*, 14971−14978.
(41) Yamamoto, K.; Kolb, D. M.; Kötz, R.; Lehmpfuhl, G. Hydrogen Adsorption and Oxide Formation on Platinum Single Crystal Electrodes. *J. Electroanal. Chem.* **1979**, *96*, 233−239.
(42) Birss, V. I.; Damjanovic, A. A Study of the Anomalous pH Dependence of the Oxygen Evolution Reaction at Platinum Electrodes in Acid Solution. *J. Electrochem. Soc.* **1983**, *130*, 1694−1699.
(43) Pourbaix, M. J. N.; Van Muylder, J.; de Zoubov, N. Electrochemical Properties of the Platinum Metals. *Platin. Met. Rev.* **1959**, *3*, 47−53.
(44) Zhan, D.; Velmurugan, J.; Mirkin, M. V. Adsorption/Desorption of Hydrogen on Pt Nanoelectrodes: Evidence of Surface Diffusion and Spillover. *J. Am. Chem. Soc.* **2009**, *131*, 14756−14760.
(45) Li, Y.; Cox, J. T.; Zhang, B. Electrochemical Responses and Electrocatalysis at Single Au Nanoparticles. *J. Am. Chem. Soc.* **2010**, *132*, 3047−3054.
(46) Holby, E. F.; Greely, J.; Morgan, D. Thermodynamics and Hysteresis of Oxide Formation and Removal on Platinum (111) Surfaces. *J. Phys. Chem. C* **2012**, *116*, 9942−9946.
(47) Henry, C. S.; Fritsch, I. Microcavities Containing Individually Addressable Recessed Microdisk and Tubular Nanoband Electrodes. *J. Electrochem. Soc.* **1999**, *146*, 3367−3373.
(48) Bond, A. M.; Luscombe, D.; Oldham, K. B.; Zoski, C. G. A Comparison of the Chronoamperometric Response at Inlaid and Recessed Disc Microelectrodes. *J. Electroanal. Chem.* **1988**, *249*, 1−14.
(49) Henry, C. S.; Fritsch, I. Microfabricated Recessed Microdisk Electrodes: Characterization in Static and Convective Solutions. *Anal. Chem.* **1999**, *71*, 550−556.